Bulletin of Earthquake Engineering
https://doi.org/10.1007/s10518-023-01755-2

ORIGINAL ARTICLE

Stochastic-based vulnerability curves for the out-of-plane seismic safety assessment of URM walls

Vasco Bernardo[1] · Alfredo Campos Costa[2] · Paulo B. Lourenço[1]

Received: 12 February 2023 / Accepted: 31 July 2023

Abstract
Earthquakes are a major cause of damage and human losses to the built environment, including cultural heritages, monumental buildings and historical centers. In the last decades, the seismic performance of buildings has received special attention due to the interest in the built heritage conservation and protection of human life, particularly with respect to masonry structures which have shown evidence of poor behavior once subjected to seismic loads. The present work contributes to the seismic safety assessment of the out-of-plane behavior of unreinforced masonry walls through a displacement-based approach, providing the capacity for different out-of-plane geometric indexes and its seismic response in different earthquake-prone regions. The analyses are conducted using a seismic probabilistic framework, considering the most common out-of-plane mechanisms, different material properties, various slenderness ratios, and a wide range of seismicity levels to cover the seismic hazard in Europe. The results presented can be useful for seismic safety assessment and to incorporate vulnerability models for seismic risk analysis.

Keywords URM walls · Out-of-plane mechanisms · Seismic probabilistic approach · Vulnerability curves · Seismic safety assessment

1 Introduction

Traditional masonry constructions are extremely vulnerable to seismic events, affecting the development of many countries around the world. This fact relies on the poor behavior of such structures when subjected to earthquakes ground motions due to the heterogeneity and anisotropy of masonry, its high specific mass and low tensile/shear strength. In addition, the absence or inappropriate connections between structural walls and between these and the adjacent horizontal diaphragm, do not allow to ensure a monolithic response of the structure and the so-called "box behavior", increasing

✉ Vasco Bernardo
vbernardo@civil.uminho.pt

[1] Department of Civil Engineering, University of Minho, Institute for Sustainability and Innovation in Structural Engineering, University of Minho, 4800-058 Guimarães, Portugal

[2] Earthquake Engineering and Structural Dynamics Unit (Structures Department), National Laboratory for Civil Engineering, Av. do Brasil 101, 1700-075 Lisbon, Portugal

Published online: 24 August 2023

significantly their seismic vulnerability. This statement is usually observed in pre-code existing masonry buildings with flexible horizontal diaphragms—most of the cases without an adequate connection between walls and floors—where their response exhibits local out-of-plane (OOP) mechanisms rather than a global response governed by the in-plane behavior, as desired.

The out-of-plane seismic response of masonry walls is one of the most complex and ill-understood areas of seismic analysis. This kind of behavior is associated to local failure and comprises the overturning of walls (Costa 2012; Ferreira 2015; Sorrentino et al. 2016; Dauda et al. 2021). Post-earthquake's observations have identified OOP collapse as one of the main failure modes in unreinforced masonry buildings (URM) and most of these occur due to inadequate design or construction. In this scope, several studies can be found in the literature, highlighting the importance of such mechanisms in the seismic performance of masonry structures (Menon and Magenes 2008; Ceran and Erberik 2013; Simões et al. 2020; Parisse et al. 2021; Dauda et al. 2021; Angiolilli et al. 2021; Gobbin et al. 2021).

Over the last decades, the implementation of codes or standards improved design and construction techniques, reducing the buildings collapse (Ghosh 1995), however, the seismic assessment of existing buildings is not trivial for practitioners. Furthermore, although current seismic safety assessment codes are oriented towards the use of nonlinear methods of analysis, the vast majority of practitioners still use linear-elastic analysis given its simplicity, which is not realistic and does not exploit the reserve capacity of the structure for moderate to high seismic intensity levels.

In Europe, the seismic safety assessment is in compliance with the specifications provided by EN 1998-3: Design of structures for earthquake resistance—Part 3: Assessment and retrofitting of buildings, hereinafter, EC8-3 (Eurocode 8 2005). It is important to point out that the current version of EC8-3 does not include the seismic verification for OOP mechanisms or assumes these as being prevented from occurring. Nevertheless, several methodologies and approaches are currently available in literature to evaluate the OOP behavior of unreinforced masonry buildings. Regarding the analytical methods currently available for OOP assessment of URM buildings, they can be divided into (1) force-based and (2) displacement-based. In brief, the former is more traditional and empirical, and comprises a static equilibrium analysis of rigid bodies, which requires the pre-definition of the damage mechanism (Giaquinta and Giusti 1985; Del Piero 1989). This approach predicts the acceleration that leads to collapse based on the strength capacity of the wall. Displacement-based methods are more accurate but less conservative and their formulation is given by the dynamic response of the pre-defined out-of-plane mechanism (Doherty et al. 2002; Jaramillo 2002; Griffith et al. 2004).

In the framework of the present study, a displacement-based approach is used to evaluate the seismic response of different OOP mechanisms purely governed by bending. The database generated for this purpose combines several values of slenderness ratios, different material properties and various axial pre-compression loads. The capacity of the walls is computed using a nonlinear force–displacement curve obtained through a mechanical-based solution, while the seismic demand is estimated by the improved capacity spectrum method for a wide range of seismicity levels in Europe, allowing to compute the so-called stochastic-based vulnerability curves. Thus, the results presented in this study—capacity *vs* demand—can be used in the OOP seismic safety assessment by the simple comparison between the capacity for a given performance level and the demand for a certain seismic intensity level. Furthermore, the results presented can be also incorporated into

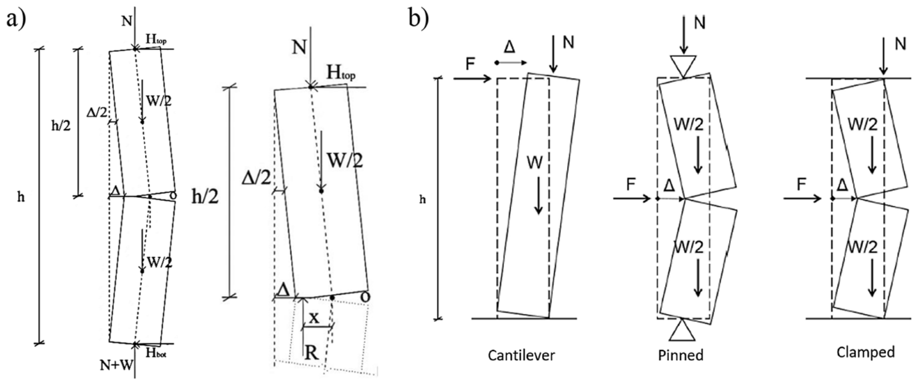

Fig. 1 OOP mechanisms of URM wall governed by simple bending **a** free body and partial diagram (adapted from Paulay and Priestly 1992), **b** different boundary conditions used in the study (adapted from Giordano et al. 2020)

vulnerability models for seismic risk analysis since the nonlinear response of the OOP is presented for different levels of seismic action.

2 Methodology and formulation

As stated before, this study is based on a displacement-based approach which consists in the dynamic response of the OOP mechanisms assumed. For this purpose, the first part of the study comprises the definition of the mechanisms, based on the principle initially proposed by Paulay and Priestly (1992), that account for a wall simply connected on the ends with a vertical resultant force at the centerline of the section, resulting in a conservative approach in the case that horizontal diaphragms are adequately connected to the walls. This methodology assumes a free body diagram with a central lateral displacement Δ as depicted in Fig. 1a, where a horizontal reaction H produces a stabilizing effect, while the vertical forces (N and W) are destabilizing for the equilibrium of the wall; R is the resulting gravity and x is the distance to the centerline. In the scope of this study, the capacity is characterized by force–displacement curves (F–Δ), computed considering the mechanical model improved by (Giordano et al. 2017, 2020). This formulation assumes that the OOP response is only governed by vertical bending and modeled through a rigid body with a nonlinear hinge located in the region with maximum bending moment. This hypothesis was discussed and validated in the literature (Brencich and Felice 2009; Parisi and Augenti 2013; Parisi et al. 2016). The nonlinear hinge that reproduces the behavior of the critical cross-section employs an analytical expression to describe the moment–curvature (M–χ) relationship for URM, defined by the elastic-brittle constitute law with zero tensile strength (Giordano et al. 2017) and expressed as a function of displacement Δ by:

$$\mathrm{M}(\Delta)=\begin{cases}\mathrm{EI}\chi=\frac{1}{12}Ebt^{3}\frac{\Delta}{L_i h}, & \Delta\le\Delta_{cr}=\frac{2N'L_ih}{Ebt^2}\\ N'\left(\frac{t}{2}-\sqrt{\frac{2N'}{9bE\chi}}\right)=N\left(\frac{t}{2}-\sqrt{\frac{2N'}{9bE\frac{\Delta}{L_ih}}}\right), & \Delta_{cr}\le\Delta\le\Delta_u=\frac{f_c^2bL_ih}{2EN'}\end{cases}\tag{1}$$

where E and f_c are, respectively, the elastic modulus and compressive strength of masonry; b is the width, t is the thickness and h is the total height of the wall, and L_i is the integration length equal to $0.25h$ according to (Giordano et al. 2017). N' is the total axial load equal to $N + W$, being N the axial pre-compression load in the wall and W the self-weight of the wall. Δ_{cr} and Δ_u correspond, respectively, to the values of the imposed displacement Δ for the cracking limit and maximum strength of the masonry due to failure of the hinges in compression.

In the next section, the nonlinear OOP capacity is computed in terms of *F-Δ* employing the above-mentioned formulation and is applied to a large database with different support configurations (see Fig. 1b), resulting in the following equilibrium expressions (see Eqs. 2, 3, 4). These boundary conditions intend to consider different interactions between the masonry walls and the lower and upper floors, including the parapet walls—*cantilever*, simple supported load bearing walls (e.g., flexible/timber floors)—*pinned* and *fixed* supported load bearing walls (e.g., continuous reinforced concrete floors) (Doherty et al. 2002; Morandi et al. 2008).

$$\text{Cantilever : F} = \frac{1}{h\alpha}\left(M - \frac{W\Delta}{2} - N\Delta\right) \tag{2}$$

$$\text{Pinned : F} = \frac{2}{h\alpha}\left(M - \frac{W\Delta}{2} - N\Delta\right) \tag{3}$$

$$\text{Fixed : F} = \frac{2}{h\alpha}\left(M - \frac{W\Delta}{4} - \frac{N\Delta}{2}\right) \tag{4}$$

where α is a non-dimensional parameter defining the position of the horizontal force F along the height of the wall.

It is important to emphasize that the formulation presented in this section was compared to others analytical models (Doherty et al. 2002; Giordano et al. 2007; Ferreira et al. 2015b) by Giordano et al. (2020) and validated against experimental test (Griffith et al. 2004; Lagomarsino 2015; Ferreira et al. 2015a; Degli Abbati and Lagomarsino 2017) for different type of masonry materials (e.g., stone, rubble and brick), evidencing its adequacy in estimating the non-linear capacity of walls subject to horizontal out-of-plane loads.

3 Derivation of the database and capacity definition

Considering the assumptions defined in the previous section, the database generated and used in the subsequently analyses comprises walls with different deterministic geometric parameters, namely height $h(m) = \{3, 4, 5, 6, 7\}$ and various values of slenderness ratio $\lambda(-) = \frac{h}{t} = \{5, 7.5, 10, 15, 20, 25\}$, which are in line with the ranges purposed by Giuffré (1996), Morandi et al. (2008) and Eurocode 6 (2018). In order to cover the large variability in the material properties of masonry in Europe, the uncertainty was propagated through Monte Carlo simulations (MCS) considering 200 random variables (r.v.) to describe the following independently mechanical parameters, with uniform distributions ranging from: compressive strength $f_c(\text{MPa}) = \{1.0 - 6.0\}$ and self-weight $\gamma\left(\text{kN/m}^3\right) = \{15.0 - 22.0\}$. The modulus of elasticity E was considered equal to $E = k * f_c$, where k factor also follows a uniform distribution ranging from 400 to 1100. It is important to point out that

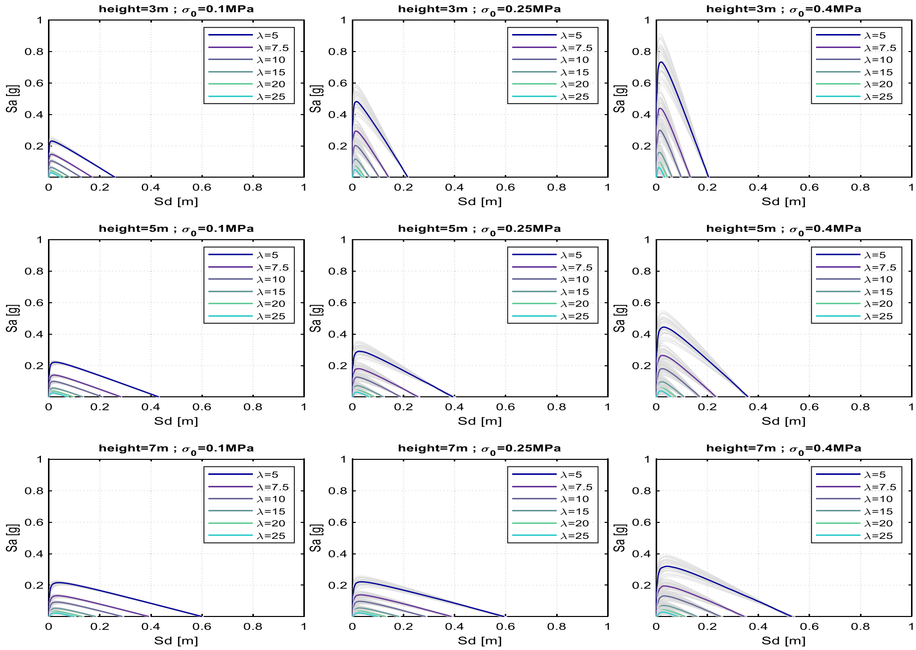

Fig. 2 Capacity curves for the OOP with cantilever boundary conditions, different slenderness values λ, heights h and pre-compression levels σ_0 as indicated

uniform distributions were assumed to consider an equal probability for each r.v. and to not introduce a bias for a given site-specific material or type of construction. Furthermore, the range of the random material properties also cover the ones purposed in NTC (2018), Candeias et al. (2020) and Lourenço and Gaetani (2022). Given the influence of the vertical load in the OOP capacity, different axial pre-compression stresses σ_0 were also adopted: $\sigma_0(\text{MPa}) = \{0.1, 0.2, 0.25, 0.30, 0.40\}$—to indirectly account for buildings with different numbers of stories, various floor types and/or different permanent/live loads. The values adopted are also in line with those considered in the investigation carried out by Morandi et al. (2008).

Figures 2, 3, 4 presents the capacity curves for the different boundary conditions assumed and for the different values of λ, $h(m) = \{3, 5, 7\}$ and $\sigma_0(\text{MPa}) = \{0.1, 0.25, 0.40\}$. The capacity curves are expressed in terms of spectral acceleration S_a and spectral displacement S_d for a single-degree-of-freedom (SDOF), as suggested by Doherty et al. (2002), which will be used in the seismic demand estimation in Sect. 4.2. The median curves are also shown for the different slenderness values adopted.

As can be readily seen, for the same values of slenderness, the OOP capacity is significantly influenced by boundary conditions and σ_0. The walls restrained at the top and bottom can explore large values of S_a and lower values of S_d, as expected, when compared to cantilever walls. Naturally, the main differences of the maximum values of S_a occurs for different values of slenderness, however, by increasing the level of σ_0 it can be noted significant differences between the maximum values of S_a for different heights, which is not so clear for lower σ_0 values.

In order to discuss more in detail the differences in the capacity achieved for the database generated, the following damage thresholds were adopted in accordance with the

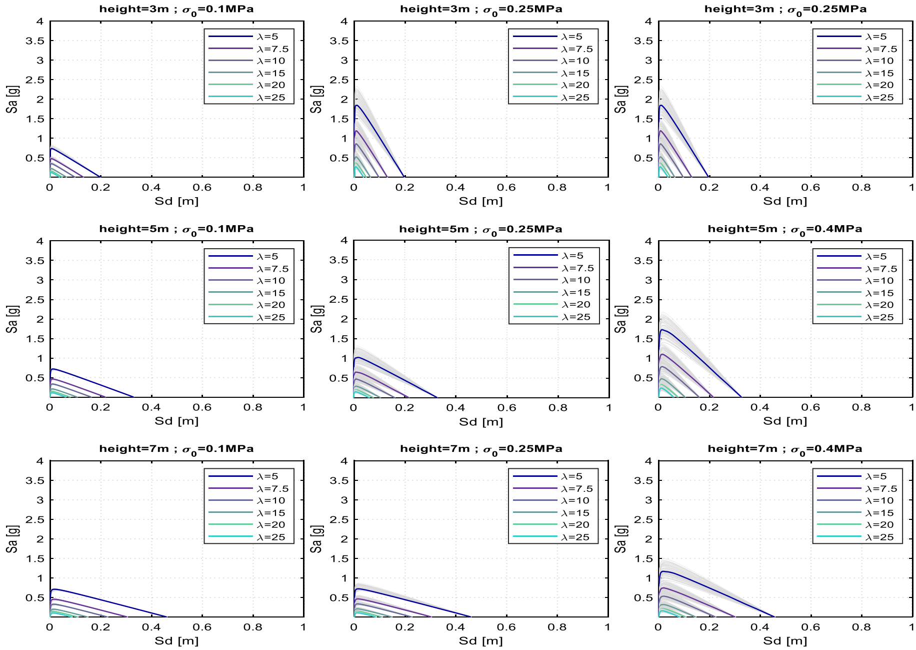

Fig. 3 Capacity curves for the OOP with pinned boundary conditions, different slenderness values λ, heights h and pre-compression levels σ_0 as indicated

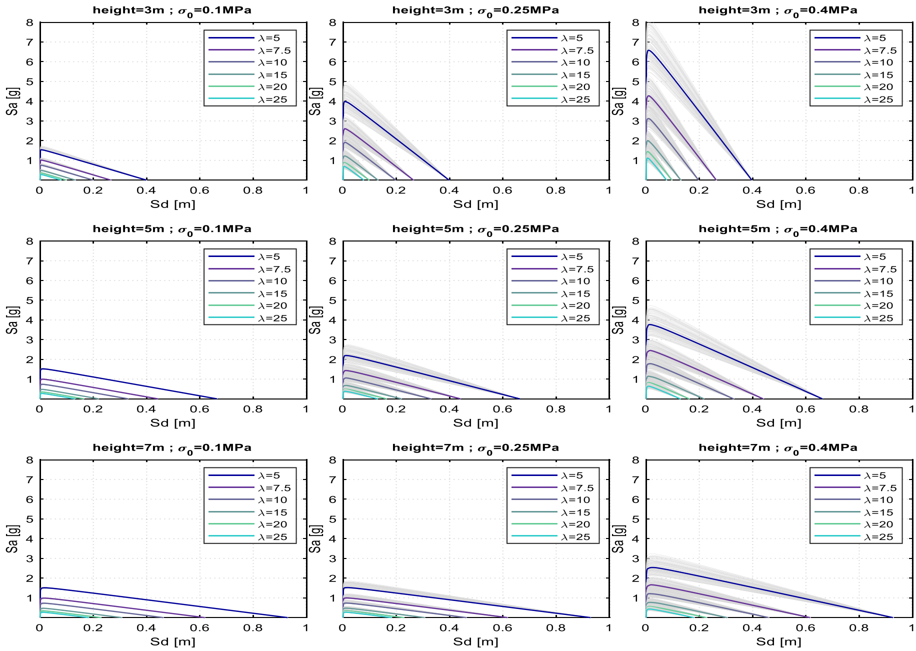

Fig. 4 Capacity curves for the OOP with fixed boundary conditions, different slenderness values λ, heights h and pre-compression levels σ_0 as indicated

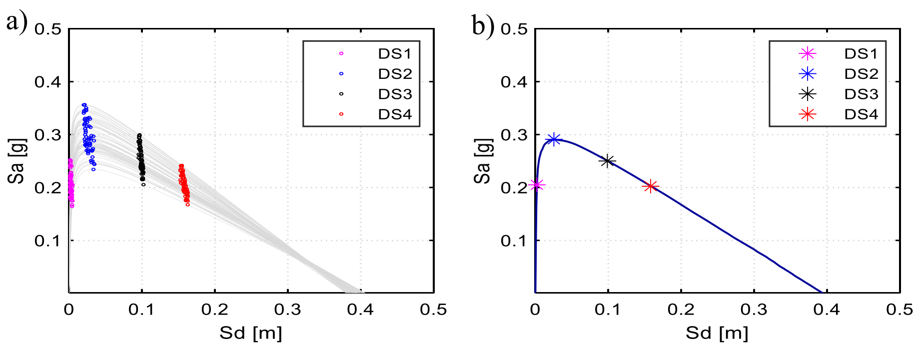

Fig. 5 Capacity curves for the OOP with cantilever boundary conditions and $h = 5.0m; \lambda = 7.5$ and $\sigma_0 = 0.25MPa$: **a** all samples and **b** median curve

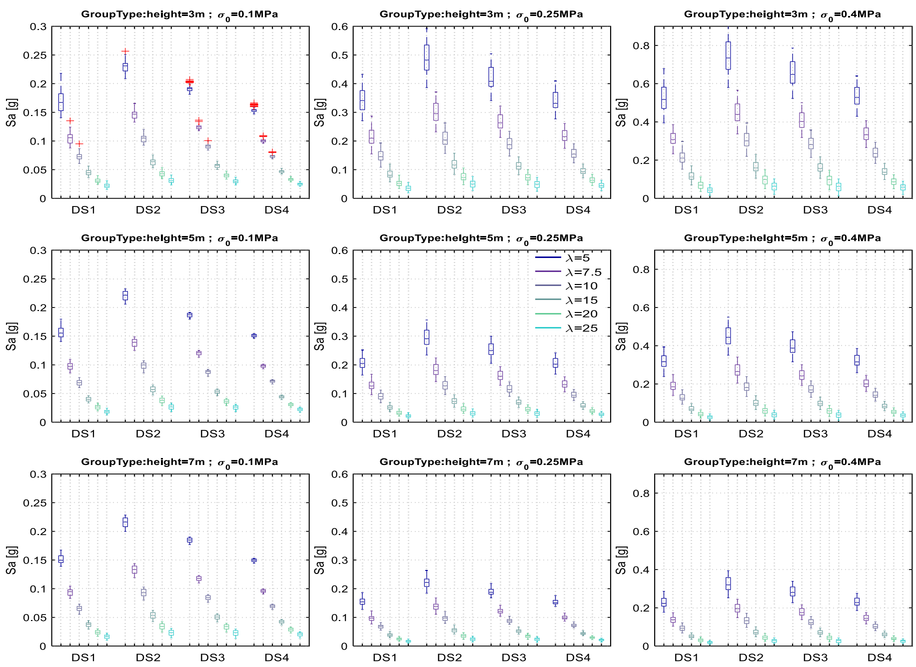

Fig. 6 Box and whisker plot for OOP S_a capacity with cantilever boundary conditions, different slenderness values λ, heights h and pre-compression levels σ_0 as indicated. Legend colors match plot colors of Fig. 2, 3 and 4

information available in literature for seismic assessment of rocking masonry structures (Lagomarsino 2015): Slight damage (DS1)—displacement achieved 70% of the maximum peak horizontal force; Moderate damage (DS2)—maximum peak strength; Severe damage (DS3)—25% of the ultimate displacement (corresponds to a null force); Near collapse (DS4)—40% of the ultimate displacement. The definition of these limit states is illustrated in Fig. 5. The results for the database are summarized in the boxplot of Figs. 6, 7 for different λ values and σ_0.

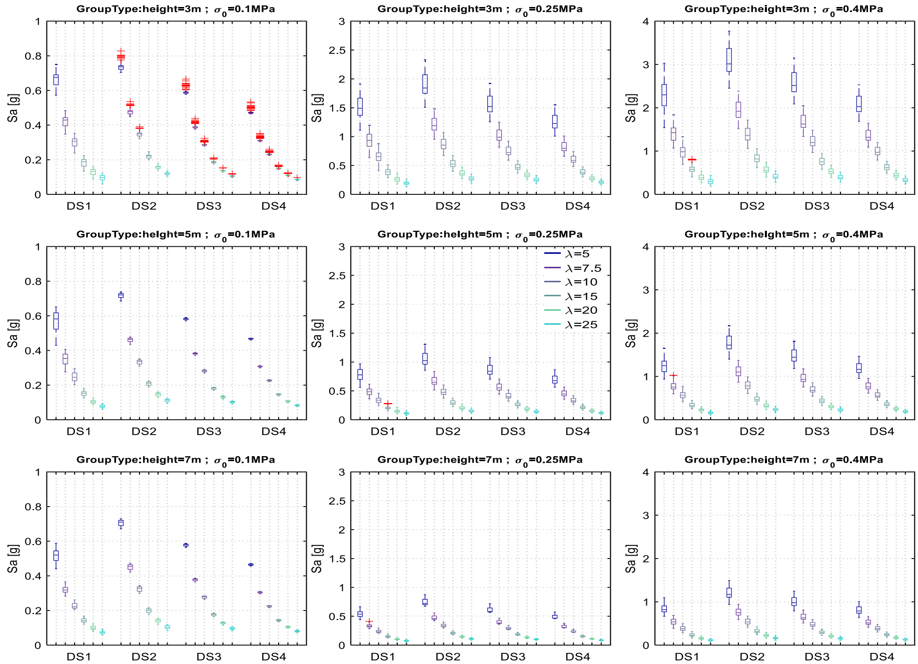

Fig. 7 Box and whisker plot for OOP S_a capacity with pinned boundary conditions, different slenderness values λ, heights h and pre-compression levels σ_0 as indicated. Legend colors match plot colors of Fig. 2, 3 and 4

Analyzing Figs. 6, 7, a large dispersion of S_a values is observed for the maximum capacity (DS2), which seems to increase from the elastic range (DS1) up to DS2, decreasing from the latter up to the ultimate displacement, as also depicted in Figs. 2, 3, 4. Note that, this conclusion can be observed independently of the slenderness and σ_0, being more pronounced as the values of σ_0 increase. It is important to mention that the dispersion in capacity β_C arises only from the variability in the material properties considered, which increases with the slenderness values. In this sense, the importance of material properties in the OOP behavior became more relevant for slender walls, while for thick walls the behavior is mostly governed by the geometry parameters. The values of β_C will be presented at the end of this section.

As previously mentioned, the structural capacity of the OOP behavior is mainly controlled by the geometry of walls (slenderness λ) and pre-compression level σ_0, where the material properties of masonry are more or less relevant depending on these variables. Thus, the relationship between the slenderness and capacity, measured in terms of spectral acceleration S_a, was computed for different levels of σ_0 and different limit states (see Figs. 8, 9, 10). Note that these figures show the median first-order power law analytical functions ($S_a = a\lambda^b$) best fitted to the entire database through a nonlinear least square method (Levenberg–Marquardt algorithm) (Moré 1978). Tables 1, 2, 3 summarizes the regression parameters (a, b) of the analytical function for different boundary conditions. The dispersion in the capacity β_C was also computed by the standard deviation of the logarithmic error between the analytical function fitted and the empirical data.

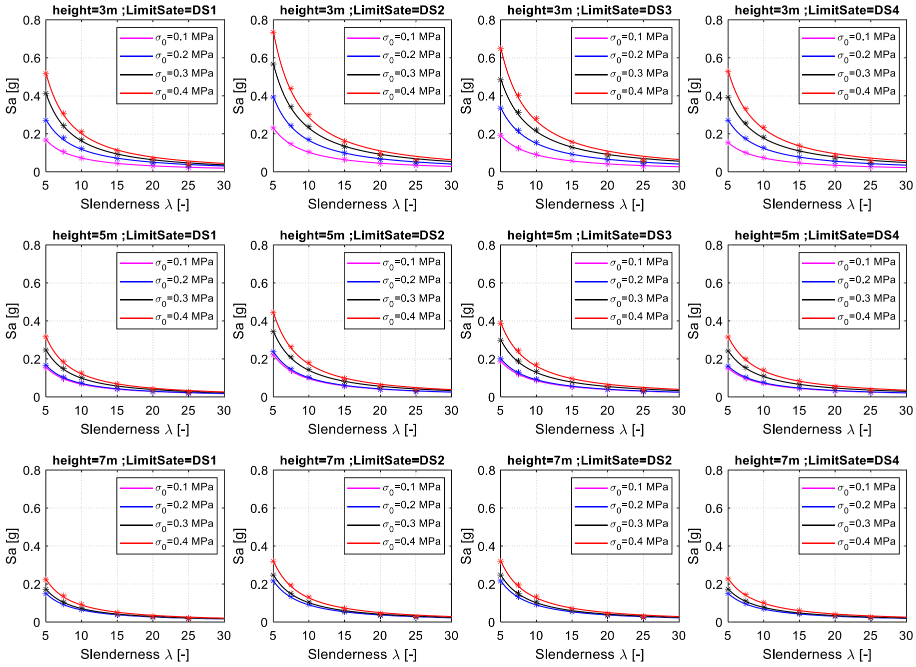

Fig. 8 Relation between different slenderness values λ and OOP S_a capacity with cantilever boundary conditions and different pre-compression levels

As can be readily seen in Figs. 8, 9, 10, the benefit of the σ_0 in the capacity of the one-way bending walls is gradually lower as the height increase, which confirms that the OOP behavior of high stories is predominantly controlled by the geometry of walls and type of connection between floors. It is also important to point out that after reaching the maximum capacity ($S_{a,max}$) the effect of σ_0 tends to decrease, given the local instability of the wall, which can also be confirmed by the slope b of the analytical functions proposed. Regarding the values of dispersion β_C (see Tables 1, 2, 3), slight differences are observed between limit states and large dispersion is attained as the σ_0 increases, namely for cantilever boundary conditions.

4 Computation of nonlinear seismic response

This section presents the seismic response of the previous database subjected to different seismicity levels in Europe. The results will be used to derive the so-called stochastic-based vulnerability curves in Sect. 5.

4.1 Seismic action and hazard definition

The seismic action was considered according to EN 1998-1 (EC8) (Eurocode 8 2004) through the representation of the horizontal elastic ground acceleration response spectrum, which is

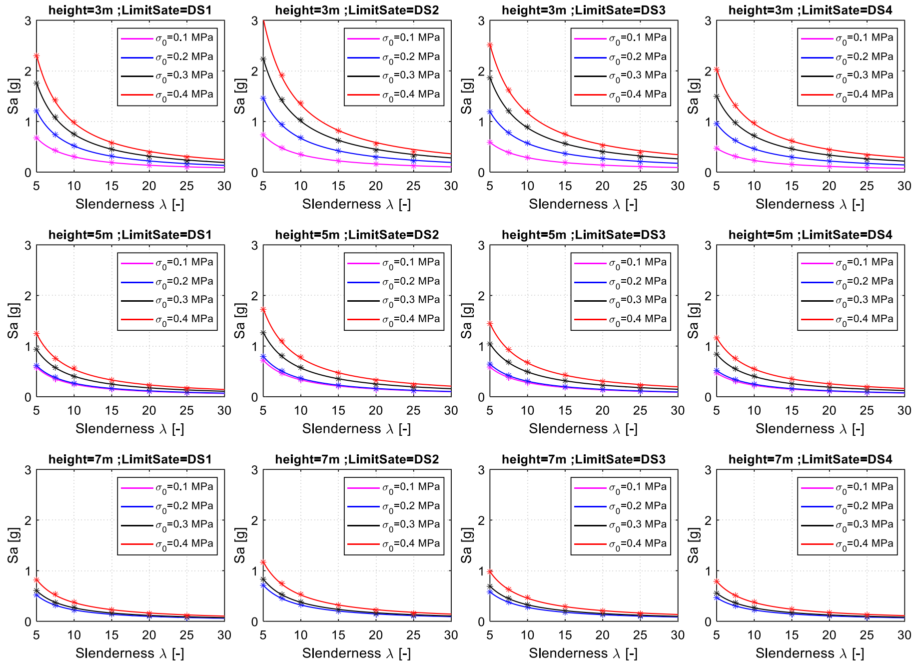

Fig. 9 Relation between different slenderness values λ and OOP S_a capacity with pinned boundary conditions and different pre-compression levels

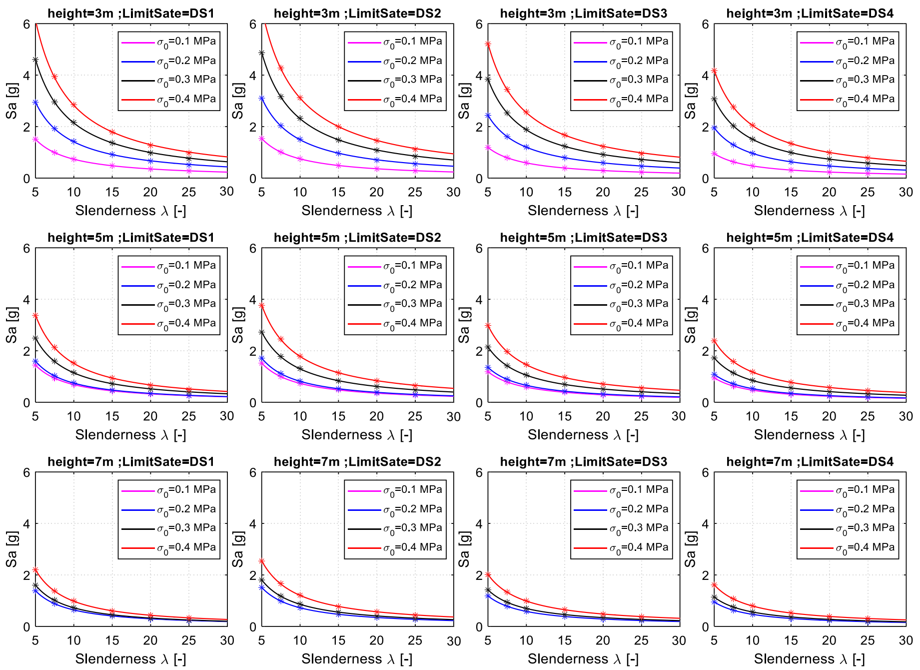

Fig. 10 Relation between different slenderness values λ and OOP S_a capacity with fixed boundary conditions and different pre-compression levels

defined by two different main seismic spectra to account for different magnitudes, epicenters, event duration and frequency content—Type 1 (high magnitude, long duration and lower frequency content) and Type 2 (moderate magnitudes, short duration and higher frequency content). The Type 1 spectrum is more suitable for earthquakes with surface magnitude $M_s > 5.5$, as occurs in most of the seismic prone regions of Italy, Greece, Turkey and Romania or offshore seismic actions in Portugal; Type 2 spectrum is more common to represent intraplate seismic scenarios, as expected in regions with moderate seismicity of northwestern or southern Europe.

Figure 11 presents different shapes for Type 1 and Type 2 spectra, where the amplification of the seismic action of the ground at the surface is indirectly accounted for various soil types (A to E) defined in EC8. The shape of EC8 spectrum is defined by the spectral acceleration $S_e(T)$ for a given return period, where T is the vibration period of the linear SDOF. The normalized EC8 spectrum can be easily constructed employing the notable points values prescribed in the Sect. 3.2.2 of the code, namely the non-dimensional parameter soil factor, that corresponds to the y-intercept (equal to 1 for bedrock—soil type A), and the corner periods in the spectral branches with constant acceleration, velocity and displacement.

The computation of different seismicity levels for the subsequent analysis was based on the concepts of probabilistic seismic hazard analysis (PSHA), which in turn are also the basis of seismic action proposed by current codes, including EC8. In brief, the PSHA was initially proposed by Cornell (1968) and is defined by hazard curves for a specific site, expressing the probability (rate per year) of a given intensity measure (IM) being exceeded. In general, the IM is expressed in terms of pseudo-spectral acceleration (S_a) or peak ground acceleration

Table 1 Regression parameters a and b and dispersion β_C: OOP with cantilever boundary conditions

Height (m)	σ_0 (MPa)	DS1			DS2			DS3			DS4		
		a	b	β	a	b	β	a	b	β	a	b	β
3	0.1	1.19	− 1.22	0.12	1.56	− 1.18	0.10	1.14	− 1.11	0.08	0.89	− 1.09	0.06
	0.2	1.99	− 1.23	0.19	3.04	− 1.27	0.17	2.27	− 1.18	0.16	1.74	− 1.15	0.14
	0.3	3.69	− 1.36	0.22	4.76	− 1.32	0.22	3.46	− 1.21	0.23	2.63	− 1.17	0.18
	0.4	4.82	− 1.38	0.27	6.78	− 1.37	0.27	5.27	− 1.29	0.32	3.95	− 1.24	0.23
4	0.1	1.04	− 1.18	0.12	1.61	− 1.22	0.10	1.18	− 1.14	0.09	0.92	− 1.11	0.07
	0.2	1.70	− 1.28	0.17	2.23	− 1.25	0.17	1.69	− 1.17	0.16	1.29	− 1.14	0.14
	0.3	2.54	− 1.32	0.22	3.62	− 1.32	0.21	2.69	− 1.23	0.22	2.03	− 1.19	0.17
	0.4	3.57	− 1.37	0.27	5.07	− 1.37	0.26	3.85	− 1.28	0.31	2.83	− 1.22	0.23
5	0.1	1.14	− 1.23	0.12	1.61	− 1.23	0.12	1.20	− 1.15	0.10	0.93	− 1.12	0.08
	0.2	1.26	− 1.25	0.17	1.81	− 1.25	0.16	1.31	− 1.16	0.15	1.01	− 1.13	0.13
	0.3	2.15	− 1.34	0.21	2.88	− 1.31	0.21	2.20	− 1.23	0.21	1.66	− 1.19	0.17
	0.4	3.02	− 1.40	0.25	4.09	− 1.37	0.25	3.08	− 1.28	0.30	2.30	− 1.23	0.22
6	0.1	1.14	− 1.25	0.14	1.71	− 1.27	0.13	1.26	− 1.18	0.12	0.97	− 1.15	0.09
	0.2	1.14	− 1.24	0.15	1.69	− 1.26	0.14	1.24	− 1.17	0.12	0.96	− 1.14	0.10
	0.3	1.69	− 1.31	0.21	2.36	− 1.30	0.21	1.81	− 1.23	0.21	1.37	− 1.18	0.17
	0.4	2.39	− 1.37	0.25	3.39	− 1.37	0.25	2.56	− 1.28	0.29	1.91	− 1.23	0.21
7	0.1	1.14	− 1.26	0.15	1.71	− 1.28	0.15	1.27	− 1.19	0.14	0.97	− 1.16	0.10
	0.2	1.14	− 1.26	0.15	1.71	− 1.28	0.15	1.27	− 1.19	0.14	0.97	− 1.16	0.10
	0.3	1.39	− 1.29	0.21	2.01	− 1.30	0.21	1.53	− 1.22	0.21	1.17	− 1.18	0.16
	0.4	1.98	− 1.35	0.25	2.86	− 1.35	0.25	2.21	− 1.28	0.28	1.65	− 1.23	0.21

Coefficients are valid for Sa measured in g

Table 2 Regression parameters a and b and dispersion β_C: OOP with pinned boundary conditions

Height (m)	σ_0 (MPa)	DS1			DS2			DS3			DS4		
		a	b	β	a	b	β	a	b	β	a	b	β
3	0.1	4.42	− 1.16	0.13	4.32	− 1.10	0.06	3.18	− 1.05	0.04	2.51	− 1.04	0.04
	0.2	8.79	− 1.23	0.15	9.20	− 1.14	0.13	6.77	− 1.08	0.12	5.36	− 1.07	0.12
	0.3	13.09	− 1.24	0.15	14.60	− 1.16	0.13	10.96	− 1.10	0.12	8.57	− 1.08	0.12
	0.4	17.34	− 1.25	0.16	20.61	− 1.19	0.14	15.13	− 1.11	0.13	11.86	− 1.09	0.12
4	0.1	4.44	− 1.21	0.13	4.38	− 1.11	0.05	3.21	− 1.06	0.03	2.54	− 1.05	0.03
	0.2	5.70	− 1.20	0.15	6.51	− 1.14	0.13	4.77	− 1.07	0.12	3.76	− 1.06	0.12
	0.3	8.78	− 1.22	0.15	10.56	− 1.16	0.13	8.01	− 1.10	0.12	6.29	− 1.09	0.12
	0.4	11.90	− 1.23	0.15	15.13	− 1.19	0.14	11.47	− 1.13	0.13	8.85	− 1.10	0.12
5	0.1	4.28	− 1.24	0.11	4.41	− 1.12	0.06	3.24	− 1.06	0.04	2.56	− 1.05	0.03
	0.2	4.32	− 1.21	0.14	5.05	− 1.15	0.12	3.68	− 1.08	0.12	2.92	− 1.07	0.11
	0.3	6.58	− 1.21	0.14	8.31	− 1.17	0.13	6.14	− 1.10	0.12	4.81	− 1.08	0.12
	0.4	8.80	− 1.21	0.15	11.72	− 1.19	0.14	8.79	− 1.12	0.13	6.83	− 1.10	0.12
6	0.1	3.79	− 1.21	0.09	4.54	− 1.14	0.06	3.31	− 1.08	0.04	2.59	− 1.06	0.03
	0.2	3.75	− 1.20	0.09	4.51	− 1.14	0.07	3.26	− 1.07	0.05	2.58	− 1.06	0.05
	0.3	5.38	− 1.22	0.14	6.55	− 1.16	0.13	4.93	− 1.10	0.13	3.88	− 1.08	0.12
	0.4	6.51	− 1.17	0.15	9.46	− 1.18	0.14	7.10	− 1.11	0.13	5.52	− 1.09	0.13
7	0.1	3.64	− 1.21	0.09	4.55	− 1.15	0.07	3.32	− 1.08	0.05	2.62	− 1.07	0.04
	0.2	3.64	− 1.21	0.09	4.55	− 1.15	0.07	3.32	− 1.08	0.05	2.62	− 1.07	0.04
	0.3	4.13	− 1.19	0.14	5.36	− 1.15	0.14	4.03	− 1.09	0.13	3.15	− 1.07	0.13
	0.4	5.41	− 1.17	0.15	7.85	− 1.18	0.14	5.88	− 1.11	0.13	4.59	− 1.09	0.13

Coefficients are valid for Sa measured in g

Table 3 Regression parameters a and b and dispersion β_C: OOP with fixed boundary conditions

Height (m)	σ_0(MPa)	DS1			DS2			DS3			DS4		
		a	b	β	a	b	β	a	b	β	a	b	β
3	0.1	8.19	− 1.06	0.06	8.25	− 1.04	0.04	6.11	− 1.02	0.03	4.88	− 1.01	0.03
	0.2	17.14	− 1.11	0.12	17.26	− 1.06	0.11	12.69	− 1.02	0.11	10.13	− 1.02	0.11
	0.3	28.25	− 1.16	0.14	27.68	− 1.08	0.11	20.22	− 1.03	0.11	16.02	− 1.03	0.11
	0.4	37.89	− 1.17	0.15	38.32	− 1.09	0.11	28.01	− 1.04	0.11	22.26	− 1.04	0.11
4	0.1	8.26	− 1.09	0.08	8.30	− 1.05	0.02	6.13	− 1.02	0.01	4.90	− 1.02	0.01
	0.2	12.45	− 1.13	0.13	12.28	− 1.07	0.11	8.99	− 1.02	0.11	7.20	− 1.02	0.11
	0.3	20.03	− 1.16	0.14	19.95	− 1.08	0.11	14.55	− 1.03	0.11	11.58	− 1.02	0.11
	0.4	26.73	− 1.17	0.13	28.01	− 1.09	0.11	20.51	− 1.04	0.11	16.28	− 1.03	0.11
5	0.1	8.33	− 1.11	0.10	8.32	− 1.06	0.03	6.14	− 1.02	0.01	4.90	− 1.02	0.01
	0.2	9.69	− 1.15	0.13	9.70	− 1.08	0.11	7.29	− 1.05	0.11	5.82	− 1.04	0.11
	0.3	15.14	− 1.17	0.13	15.45	− 1.08	0.11	11.32	− 1.03	0.11	9.00	− 1.03	0.11
	0.4	19.99	− 1.17	0.13	21.82	− 1.09	0.11	15.88	− 1.04	0.11	12.62	− 1.03	0.11
6	0.1	8.36	− 1.10	0.08	8.38	− 1.06	0.03	6.18	− 1.02	0.01	4.92	− 1.02	0.01
	0.2	8.36	− 1.10	0.09	8.33	− 1.06	0.04	6.16	− 1.02	0.03	4.90	− 1.02	0.03
	0.3	12.52	− 1.14	0.13	12.36	− 1.07	0.11	9.09	− 1.03	0.11	7.24	− 1.03	0.11
	0.4	17.73	− 1.17	0.14	17.39	− 1.08	0.11	12.81	− 1.03	0.11	10.17	− 1.03	0.11
7	0.1	8.39	− 1.12	0.11	8.38	− 1.06	0.03	6.18	− 1.02	0.01	4.92	− 1.02	0.01
	0.2	8.39	− 1.12	0.11	8.38	− 1.06	0.03	6.18	− 1.02	0.01	4.92	− 1.02	0.01
	0.3	10.30	− 1.15	0.14	10.20	− 1.07	0.12	7.43	− 1.03	0.12	5.95	− 1.03	0.12
	0.4	14.57	− 1.17	0.14	14.55	− 1.08	0.11	10.66	− 1.03	0.11	8.50	− 1.03	0.11

Coefficients are valid for Sa measured in g

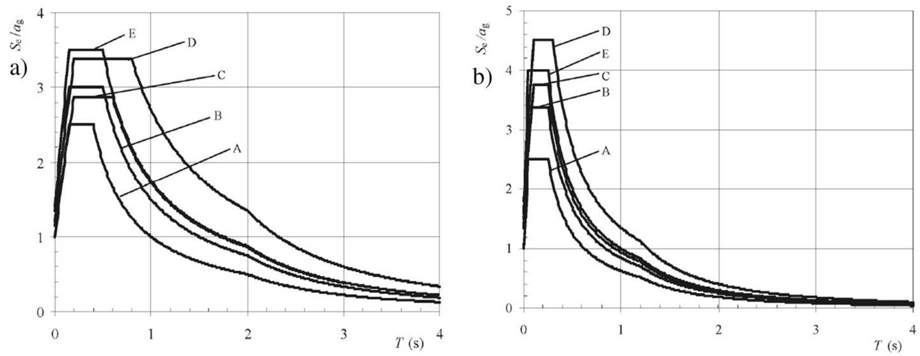

Fig. 11 Eurocode 8 elastic response spectrum: **a** Type 1 and **b** Type 2

(PGA) values. An extended state-of-the-art review of PSHA can be consulted in McGuire (2008), or more recently Gerstenberger et al. (2020).

The reference seismic action defined in EC8 is associated with a reference probability of exceedance in 50 years or a reference return period $T_{r,ref}$. This probability of exceedance is generally related to the performance level of the structure corresponding to a given limit state. In the case of EC8, the reference seismic action corresponds to a $T_{r,ref} = 475$ years or a 10% probability of exceedance in 50 years, associated to the ultimate limit state. In the scope of this study, several values of reference peak ground accelerations PGA_{ref} were considered to cover most of the variability found in Europe $PGA_{ref}(g) = \{0.05, 0.1, 0.2, 0.3, 0.4\}$. Note that, these values of PGA_{ref} are associated to the 475-years reference return period. In order to estimate the response of a given structure for different return periods $T_{r,i}$, the PGA can be computed by $PGA = PGA_{ref}(T_{r,ref}/T_{r,i})^{-1/k_1}$, where k_1 is the slope of the first-order power law function fitted to the hazard curve (Cornell 1968; Vamvatsikos 2013). The coefficient k_1 depends on the seismicity in the region, being considered the following values $k_1 = \{1.0, 1.5, 2.0, 2.5, 3.0, 3.5\}$. It is important to point out that the values selected for the PGA_{ref} and k_1, shown in Fig. 12, aim to characterize different seismic regions in Europe on the basis of SHARE project (Woessner et al. 2015). Nevertheless, the results and conclusions presented are valid for other regions because it is linked only to PGA_{ref} and k_1 and not seismic zonation itself.

4.2 Seismic demand estimation

The structural response of the previous database of walls was estimated by using the improved Capacity Spectrum Method (CSM). This method corresponds to one of the most used in the evaluation of the seismic performance of structures, and it allows determining the performance point (seismic demand) of a given structure, characterized by a capacity spectrum (see Sect. 3), against a specific seismic action (see Sect. 4.1), defined through a response spectrum (action effect or demand). Both capacity spectrum and response spectrum should be defined in the ADRS (Acceleration Displacement Response Spectrum) format. The fundamentals of CSM are described in Comartin et al. (2000) "Seismic Evaluation and Retrofit of Concrete Buildings" and FEMA-440 "Improvement of Nonlinear Static Seismic Analysis Procedures" (FEMA 2005).

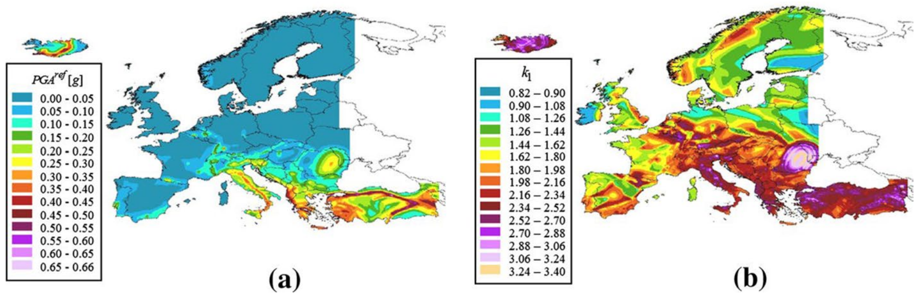

Fig. 12 Seismic hazard maps for Europe: **a** PGA at the 475-years return period; **b** k_1 coefficient for first-order power law approximation for the seismic hazard, adapted from (Woessner et al. 2015; Gkimprixis et al. 2019)

The performance point is obtained by intersecting the capacity spectrum of a given structure with the response spectrum for the seismic action under analysis and for the same level of dissipated energy, i.e., for the same damping level. As such, an iterative process was used according with (FEMA 2005) to determine the point where the capacity curve and the response spectrum intersect at the same level of dissipated energy, which implies that the damping resulting from the capacity spectrum also corresponds to the reduction factor of the seismic action response spectrum.

This procedure was employed on the database presented in Sect. 3 and several seismic intensity levels, i.e., various response spectra corresponding to earthquakes with different probabilities of occurrence (different return periods). Thus, the study considered the seismic action presented in previous section and the following different seismicity levels $T_r(years) = \{10, 20, 50, 95, 225, 475, 975, 1100, 2475, 3500, 5000\}$. Figure 13 exemplifies the performance points for different seismicity and considering a given median curve of the database generated—height = 5.0m (λ=10) —with different boundary conditions. Note that, the seismic action is represented by the initial response spectrum with 5% damping and $k_1 = 1.5$. As it can be seen, the structure with cantilever boundary conditions, from Fig. 13a, b, attained the slight damage limit state (DS1) for T_r lower than 225 years (PGA_{ref} = 0.1 g) and 50 years (PGA_{ref} = 0.3 g); for pinned boundary conditions the slight limit state (DS1) is only reached for T_r higher than 1100 years (PGA_{ref} = 0.1 g) and 475 years (PGA_{ref} = 0.3 g). Although these differences between the two mechanisms are expected, they highlight the importance of restricting horizontal displacement (e.g., tie rods) on the seismic performance of the structures.

5 Derivation of stochastic-based vulnerability curves

Stochastic-based vulnerability curves presented in this section represents the relationship between the seismic response of a given typology of wall (defined by its slenderness, σ_0 and boundary conditions) for different recurrence periods, as a function of a certain seismicity and seismic intensity level. The vulnerability curves were derived through cloud analysis for several return periods and by fitting a nonlinear regression model to the response of the analyzed typologies following the procedures described below, which make the outcomes valid for the seismic verification considering any performance level (limit state).

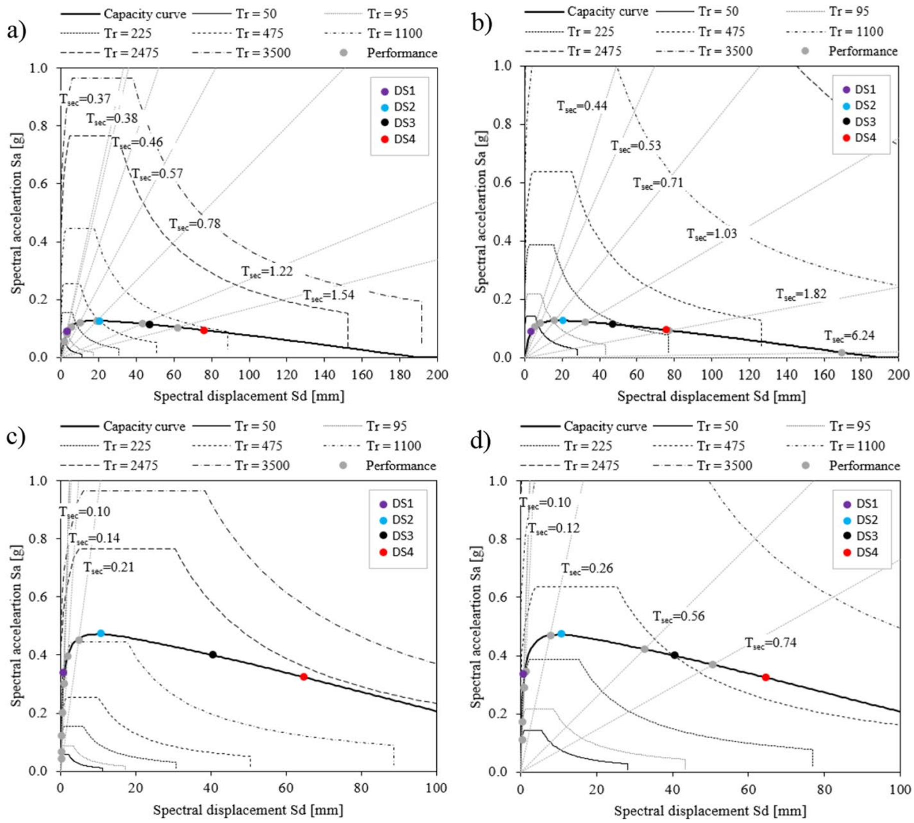

Fig. 13 Performance points for median capacity spectrum for structure with height = 5.0 m (λ = 10), different seismicity ($k_1 = 1.5$) and ground type A: **a** and **b** cantilever boundary condition and $PGA_{ref} = 0.1$g and 0.3g, respectively; **c** and **d** pinned boundary condition and $PGA_{ref} = 0.1$g and 0.3g, respectively

The process for deriving the vulnerability curves employed the methodology described in the previous section by considering the spectral acceleration S_a as the engineering demand parameter (EDP). Thus, for each return period T_r the performance point of every single structure subjected to a given seismicity was estimated. This procedure was repeated for the entire database. Figure 14a, b show the resulting fragility curves for two of the adopted return periods, considering a given typology of wall and a certain seismic action. Both the empirical cumulative density function (CDF) and analytical function expressed by a LogN distribution are depicted. After demand values of S_a were obtained for the entire range of T_r adopted, analytical curves were best fitted to the data (cloud analysis) using a nonlinear least square method (Levenberg–Marquardt algorithm) (Moré 1978) over the range of T_r up to reach the ultimate capacity in terms of S_a, as can be seen in Fig. 14c, d. The grey dots plotted in these figures represent the response of the wall for certain selected return periods, i.e., T_r (years) = {10, 50, 95, 225, 475, 975}, by considering the variability in the material properties (see Sect. 3) for the wall typology exemplified. The analytical function adopted, computed in Fig. 14c, d for the 16th, 50th and 84th quantiles, is defined by a two-term exponential model: $S_a(T_r) = ae^{bT_r} + ce^{dT_r}$, where a, b, c, d are the regression coefficients best fitted to the empirical data, which depends on the response of the

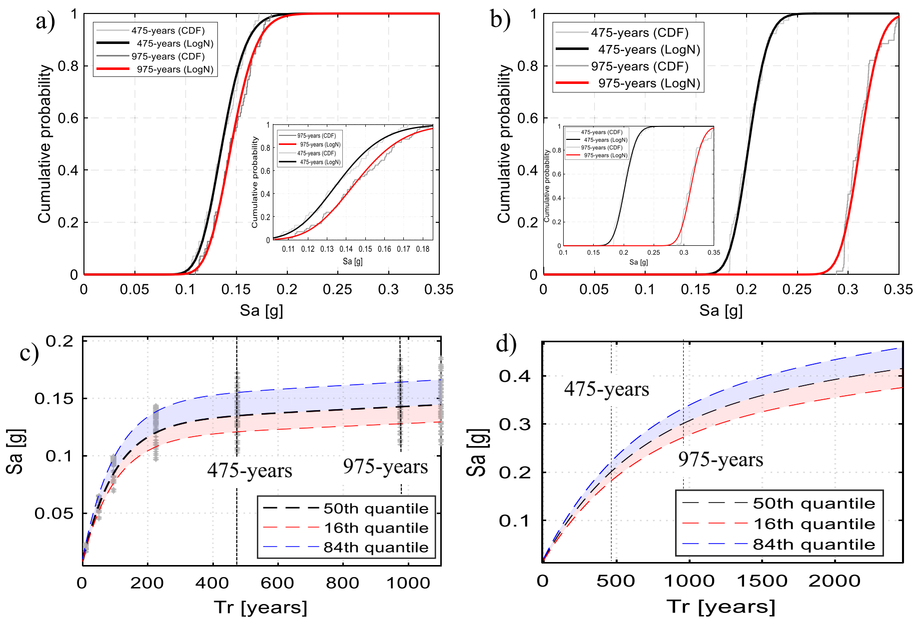

Fig. 14 Example of the analytical functions fitted to data for structures with height = 5.0 m (λ = 10, $\sigma_0 = 0.3\mathrm{MPa}$), seismicity ($k_1 = 1.5, PGA_{ref} = 0.1\mathrm{g}$), ground type A and different T_r.—cantilever and pinned boundary condition respectively: **a** and **b** fragility curves; **c** and **d** vulnerability curves

structures for a given seismicity and seismic hazard. Therefore, the relation between the spectral acceleration demand S_a and return period T_r can be described by the proposed model as a function of seismic action. As can be readily seen from the example in Fig. 14, the values of the Sa demand increase as Tr increases until the maximum capacity of the wall is reached. For instance, Fig. 14a shows the Sa demand values increasing with the Tr considered, since the maximum strength capacity of the wall is about 0.16 g-0.18 g (see Fig. 2). Moreover, the large capacity of the walls with pinned boundary conditions allows to explore higher levels of seismicity compared to the cantilever walls. This discussion will be addressed in more detail at the end of this section.

The stochastic-based vulnerability curves proposed can be used to estimate the seismic demand of a given wall typology subjected to a specific seismic intensities and seismic hazard, which confronted with its OOP structural capacity provided in Sect. 3 can be used for seismic safety assessment by: (1) computation of capacity as a function of wall typology—slenderness, pre-compression level and support conditions; (2) for the same wall typology and a certain seismic action level (or performance level) estimation of the seismic demand; (3) comparison between the capacity and demand to conclude on the seismic safety assessment procedure (Figs. 15, 16, 17, 18, 19, 20).

Figures 15, 17, 19 compares the vulnerability curves for selected wall typologies under different pre-compression levels and boundary conditions, subjected to different seismic hazard and intensities. For convenience, the curves are presented with a log scale in the x-axis. The dispersion in demand β_D is depicted in Figs. 16, 18, 20.

As can been seen from the graphs of vulnerability curves (Figs. 15, 17, 19) the response is mostly affected by the slenderness and support conditions, as expected. Axial

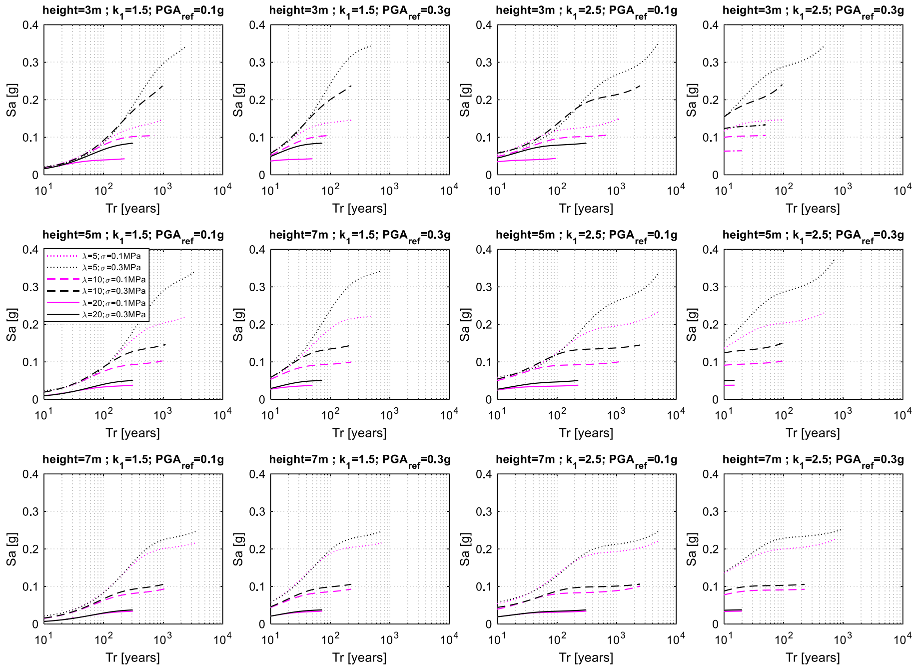

Fig. 15 Example of stochastic-based vulnerability curves for different seismicity, slenderness and pre-compression levels: cantilever boundary conditions

compression σ_0 also plays an important role in the wall's response, but its effects tend to decrease with the increasing of the height. For the walls with cantilever boundary conditions (no top restraint), Fig. 15, the slenderness values influence the final response of the walls, i.e., the achieved return period (or performance level) for the same seismic hazard and intensity is lower for the slenderer ones (lower capacity). This fact is also observed in the other support conditions, however, for the cantilever support, it is more evident since the OOP bending mechanism depends essentially on the geometry of the walls. Considering the variation of the slope k_1 of the hazard curve, it is observed for the same values of the demand S_a, greater values of achieved return period (lower rate per year) as the k_1 values increase, which reflects the larger exponential decay of the rate per year for higher slope values on the hazard curve for a certain seismicity and conditioned by a given value of PGA. Naturally, for the same seismic hazard but higher seismic intensity levels, the expected demand is larger for the same return period, which means that structures reach a certain performance level more quickly than when subjected to lower intensity levels.

Regarding the typologies with pinned (Fig. 17) and fixed (Fig. 19) supports conditions, the previous conclusions are also confirmed, however, given the increase in the structural capacity of these ones, some structures do not reach the ultimate capacity, where in some cases a similar response (demand) is obtained for lower intensity levels (e.g., $PGA_{ref} = 0.1g$), even for the slenderer walls. This is more evident for higher k_1 values, according to the justification given above, and in particular for fixed boundary conditions with higher capacity strength. Note that this observation tends to be less evident for increasing levels of intensity, as the structures enter into another domain of the capacity

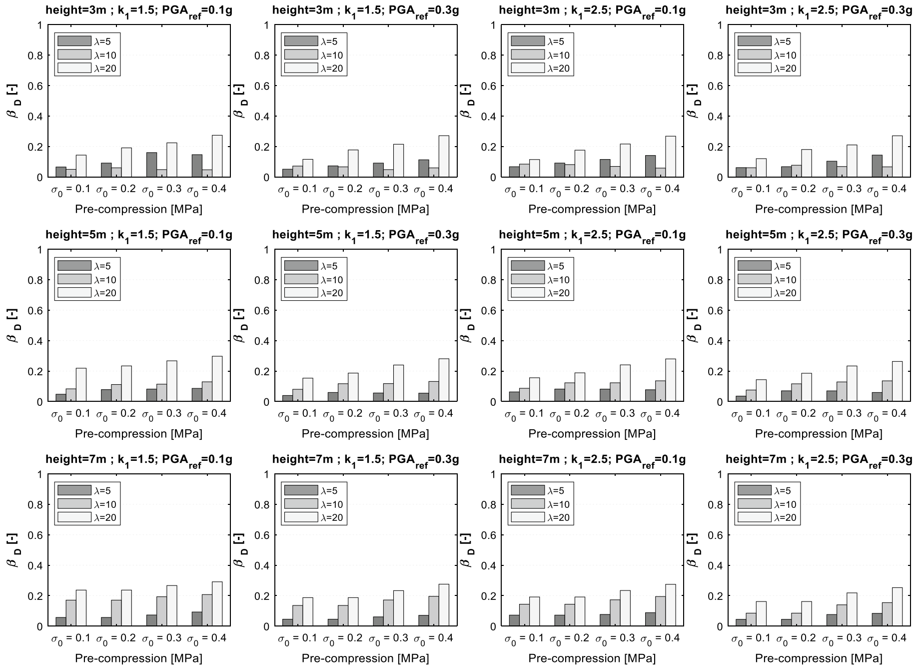

Fig. 16 Seismic demand dispersion for different seismicity, slenderness and pre-compression levels: cantilever boundary conditions

curve, i.e., approaching the ultimate capacity strength, where parameters such as geometry, material properties, and axial loading become more relevant to the nonlinear response.

Finally, the dispersion in the demand β_D (Figs. 16, 18, 20) shows, in general, large values for the cantilever boundary conditions typology, which seems to increase with the slenderness values and σ_0. This larger dispersion results essentially from the dispersion in the material properties considered, where its variability is more relevant for slenderer walls, while for lower slenderness values the behavior/response is mostly governed by the geometry of the wall. The same is verified for the effect of axial load, which has a greater influence on slender walls as also discussed in the results of Sect. 3. On the other hand, for fixed and fixed supports, although there is a slight variation with increasing values of slenderness and σ_0, it is not so evident as the cantilever support typology. This finding again reflects that the geometry of the walls has a greater influence compared to the variability of the material properties as the kinematic constraints at the supports increase. Moreover, it is also observed that the dispersion values tend to be higher for the cases in which the higher capacity of the walls is exploited, evidencing that the dispersion in the response increases as the maximum OOP capacity strength of the wall approaches (non-linear behavior).

The application of the proposed methodology is summarized in the following main steps: (1) building survey (e.g., building geometry, walls thickness, pre-compression level); (2) definition of the OOP mechanism as a function of the boundary conditions; (3) definition of the limit state to be verified; (4) estimation of the seismic capacity in terms of S_a -capacity (see Figs. 8, 9, 10); (5) estimation of the seismic demand in terms of S_a-demand (see Figs. 15, 17, 19) as a function of the seismic region, return period (associated to

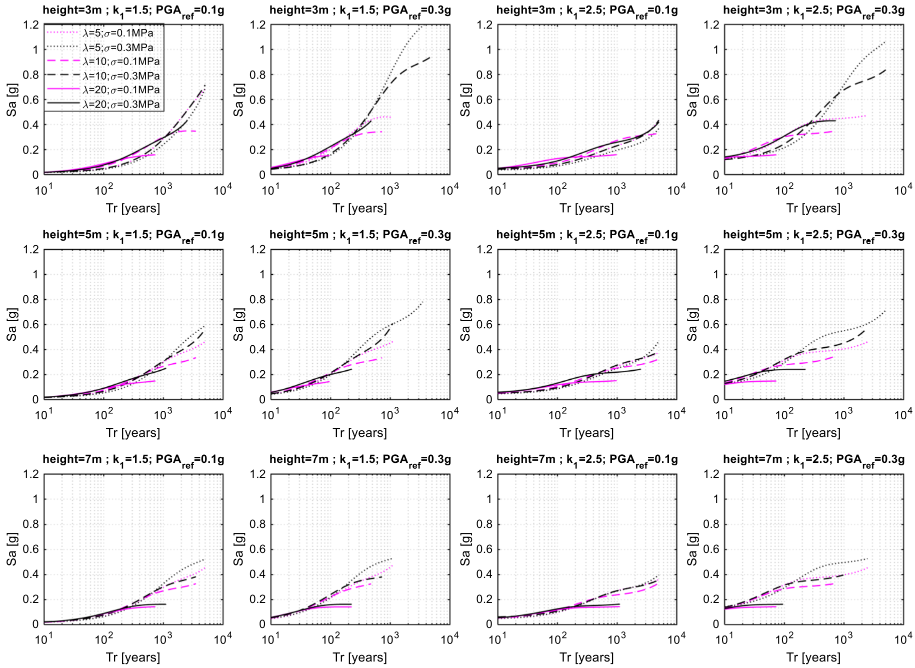

Fig. 17 Example of stochastic-based vulnerability curves for different seismicity, slenderness and pre-compression levels: pinned boundary conditions

the limit state evaluated) and OOP mechanism; (6) comparison of the S_a-capacity and S_a -demand values computed in (4) and (5), respectively, in order to conclude the seismic safety assessment procedure for the considered mechanism. For instance, in the case of a given wall (cantilever mechanism, h = 3.0 m, λ=10, σ_0=0.3MPa) under a certain seismicity (PGA_{ref}=0.1g, k_1=2.5) and for a 475-years return period (corresponding to the ultimate capacity strength verification—DS2 limit state), the median value of Sa-capacity is approximately 0.22 g (see Fig. 8) while the Sa-demand is about 0.20 g (see Fig. 15), therefore this particular case verifies the seismic safety.

6 Final comments and conclusions

The present study evaluated the out-of-plane (OOP) response of unreinforced masonry walls governed by bending and subjected to several seismicities and seismic hazard levels, in order to cover different seismic zones in Europe. For this purpose, a wall typology database was generated by combining several slenderness ratios, different material properties (using Monte Carlo simulation), various axial pre-compression loads and the

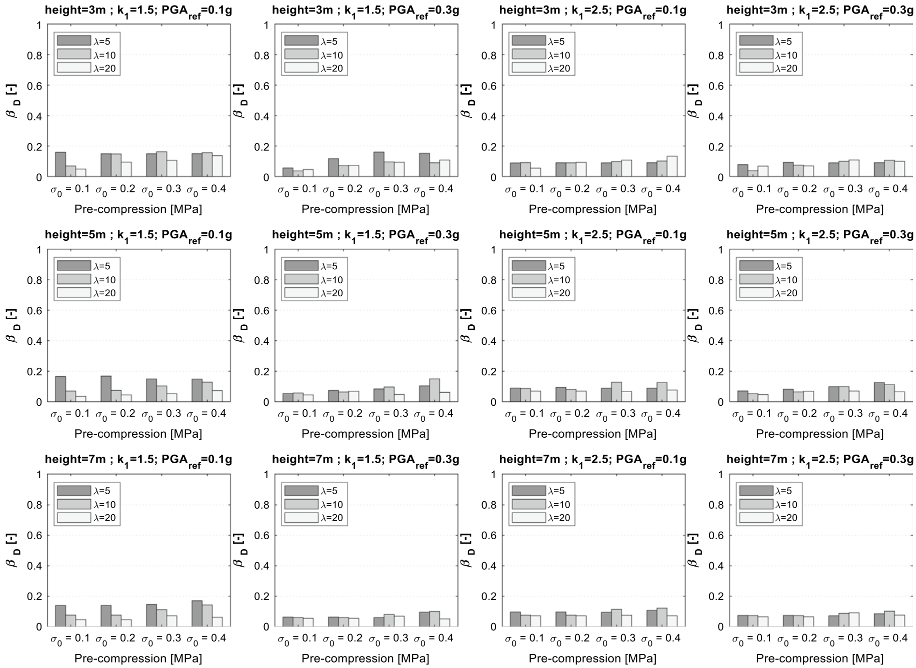

Fig. 18 Seismic demand dispersion for different seismicity, slenderness and pre-compression levels: pinned boundary conditions

following mechanisms: (1) rigid body with a *cantilever* configuration; (2) system of rigid bodies with *pinned* support conditions and (3) system of rigid bodies with *fixed* supports. These mechanisms intended to consider different interactions between the masonry walls and their lower and upper floors.

The capacity of the walls was estimated by employing a mechanical-based formulation that accounts for the nonlinear behavior in the wall cross-section through an elastic-brittle constitutive law (no tensile strength) for uncracked and cracked conditions, which allowed to compute nonlinear force–displacement capacity curves for the database generated. Based on these results, analytical functions were provided that express the OOP capacity in terms of spectral acceleration (S_a) as a function of geometric parameters, axial loads and accounting the randomness in the material properties. The main findings showed that the OOP capacity is mainly influenced by wall geometry, axial loading and support conditions, compared to variability in material properties, however, with increasing slenderness values the level of pre-compression becomes less important and the aleatory uncertainty in the material properties became more relevant to the capacity, resulting in a greater dispersion in this case.

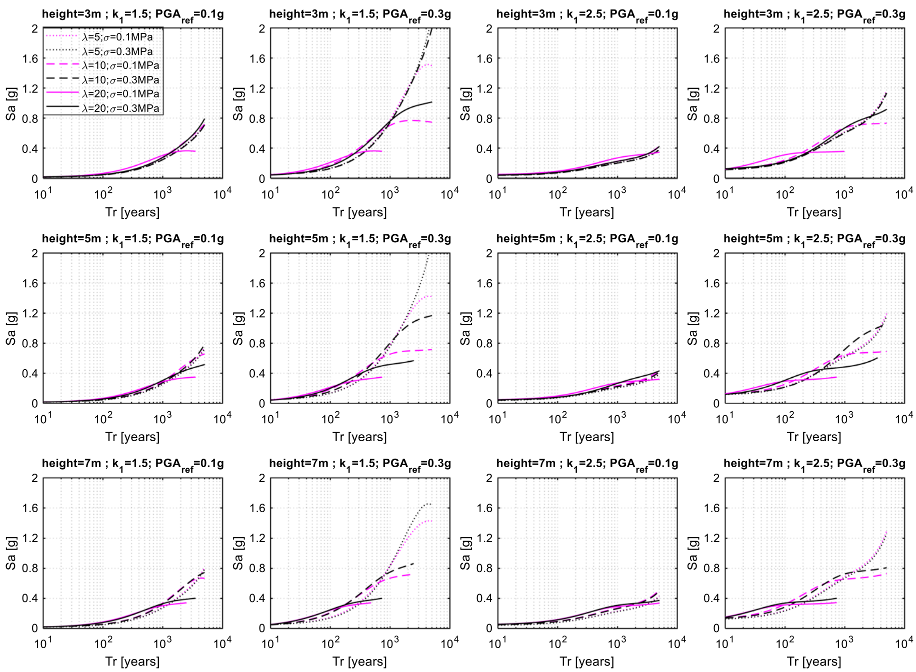

Fig. 19 Example of stochastic-based vulnerability curves for different seismicity, slenderness and pre-compression levels: fixed boundary conditions

Taking advantage of the previous results, the seismic performance was evaluated for the entire database under different seismicity levels allowing to derive the so-called stochastic-based vulnerability curves, which provide a relationship for the seismic response of a given typology of wall as a function of a certain seismicity and seismic hazard. According to the results obtained, the walls response is mostly governed by their geometry and supports constraints, while the influence of axial load depends essentially on the seismicity, i.e., for lower seismic intensities levels the axial load is not so relevant to the demand, even for lower slenderness values, while for moderate to high seismicities, the axial load importance increases as the response reaches the maximum strength of the wall capacity. Regarding the dispersion in demand, large values are obtained for the cantilever mechanism with a tendency to increase with the slenderness values and axial load, where the randomness in the material properties are more relevant for the wall's response. For the other mechanisms, dispersion tends to be greater for cases where the higher capacity of the walls is exploited.

Finally, the results presented in this study are useful for seismic safety assessment of OOP behavior, as they provide simple relationships to compute the capacity and the seismic demand in compliance with the seismic action in the code. The results can be also incorporated in vulnerability models for seismic risk analysis or code calibration of new standards given the database response in different seismic regions and earthquake recurrence periods.

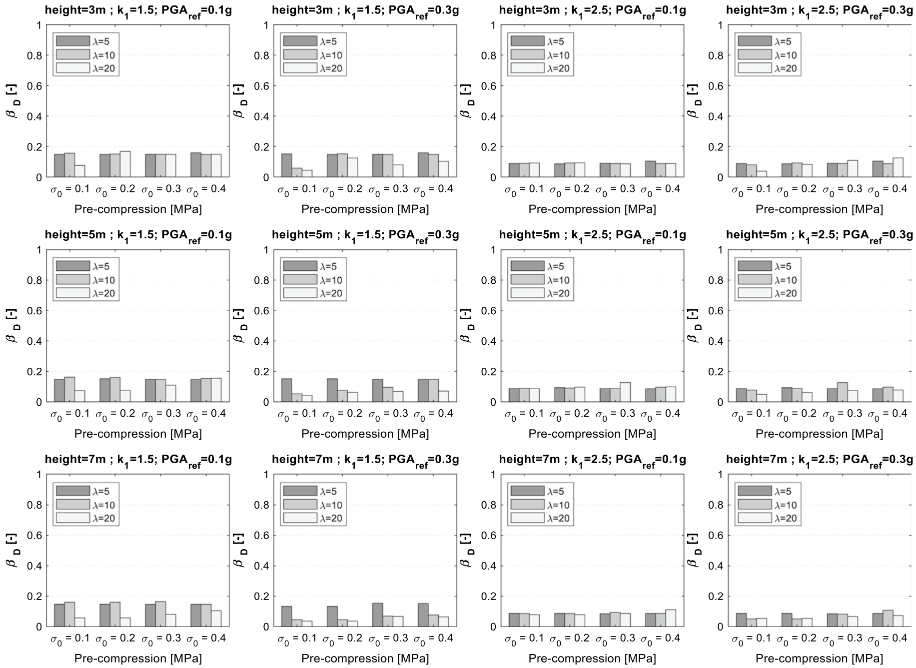

Fig. 20 Seismic demand dispersion for different seismicity, slenderness and pre-compression levels: fixed boundary conditions

Nevertheless, special attention is needed to extrapolate the proposed vulnerability curves to the level of building floors, since they are not filtered by the dynamic response of the structure. In this sense, future research should further develop the presented approach to derive vulnerability curves in different MDOF systems and considering other OOP mechanisms.

Funding Open access funding provided by FCT|FCCN (b-on). This study was funded by the STAND4HERITAGE project that has received funding from the European Research Council (ERC) under the European Union's Horizon 2020 research and innovation program (Grant agreement No. 833123), as an Advanced Grant. This work was also partly financed by FCT/MCTES through national funds (PIDDAC) under the R&D Unit ISISE under reference UIDB/04029/2020.

Availability of data and materials Not applicable.

Declarations

Conflicts of interest No potential conflict of interest was reported by the authors.

References

Angiolilli M, Lagomarsino S, Cattari S, Degli Abbati S (2021) Seismic fragility assessment of existing masonry buildings in aggregate. Eng Struct 247:113218. https://doi.org/10.1016/j.engstruct.2021.113218

Brencich A, de Felice G (2009) Brickwork under eccentric compression: experimental results and macroscopic models. Constr Build Mater 23:1935–1946. https://doi.org/10.1016/j.conbuildmat.2008.09.004

Candeias P, Correia A, Costa AC, et al (2020) General aspects of the application in Portugal of Eurocode 8—Part 3—Annex C (Informative)—Masonry Buildings [in Portuguese]. Revista Portuguesa de Engenharia de Estruturas

Ceran HB, Erberik MA (2013) Effect of out-of-plane behavior on seismic fragility of masonry buildings in Turkey. Bull Earthq Eng 11:1775–1795. https://doi.org/10.1007/s10518-013-9449-0

Comartin CD, Niewiarowski RW, Freeman SA, Turner FM (2000) Seismic evaluation and retrofit of concrete buildings: a practical overview of the ATC 40 document. Earthq Spectra 16:241–261. https://doi.org/10.1193/1.1586093

Cornell CA (1968) Engineering seismic risk analysis. Bull Seismol Soc Am 58:1583–1606. https://doi.org/10.1785/BSSA0580051583

Costa AA (2012) Seismic assessment of the out-of-plane performance of traditional stone masonry walls (PhD Thesis). Faculty of Engineering, University of Porto. FEUP

Dauda JA, Silva LC, Lourenço PB, Iuorio O (2021) Out-of-plane loaded masonry walls retrofitted with oriented strand boards: numerical analysis and influencing parameters. Eng Struct 243:112683. https://doi.org/10.1016/j.engstruct.2021.112683

Degli Abbati S, Lagomarsino S (2017) Out-of-plane static and dynamic response of masonry panels. Eng Struct 150:803–820. https://doi.org/10.1016/j.engstruct.2017.07.070

Del Piero G (1989) Constitutive equation and compatibility of the external loads for linear elastic masonry-like materials. Meccanica. https://doi.org/10.1007/BF01559418

Doherty K, Griffith MC, Lam N, Wilson J (2002) Displacement-based seismic analysis for out-of-plane bending of unreinforced masonry walls. Earthq Eng Struct Dyn 31:833–850. https://doi.org/10.1002/eqe.126

Eurocode 6 (2018) European Standard EN 199-1-1: design of masonry structures—Part 1-1: general rules for reinforced and unreinforced masonry structures

Eurocode 8 (2005) European Standard EN 1998–3:2005: design of structures for earthquake resistance—Part 3: assessment and retrofitting of buildings. Comite Europeen de Normalisation

Eurocode 8 (2004) European Standard EN 1998-1:2004: design of structures for earthquake resistance—Part 1: General rules, seismic actions and rules for buildings. Comite Europeen de Normalisation

FEMA (2005) Improvement of Nonlinear Static Seismic Analysis Procedures. FEMA 440, Federal Emergency Management Agency, Washington

Ferreira T (2015) Out-of-plane seismic performance of stone masonry walls: experimental and analytical assessment (PhD Thesis). University of Aveiro, Aveiro, Portugal

Ferreira TM, Costa AA, Arêde A et al (2015a) Experimental characterization of the out-of-plane performance of regular stone masonry walls, including test setups and axial load influence. Bull Earthq Eng 13:2667–2692. https://doi.org/10.1007/s10518-015-9742-1

Ferreira TM, Costa AA, Vicente R, Varum H (2015b) A simplified four-branch model for the analytical study of the out-of-plane performance of regular stone URM walls. Eng Struct 83:140–153. https://doi.org/10.1016/j.engstruct.2014.10.048

Gerstenberger MC, Marzocchi W, Allen T et al (2020) Probabilistic seismic hazard analysis at regional and national scales: state of the art and future challenges. Rev Geophys 58:1. https://doi.org/10.1029/2019RG000653

Ghosh SK (1995) Observations on the performance of structures in the Kobe earthquake of January 17, 1995. PCI J 40:14–22. https://doi.org/10.15554/pcij.03011995.14.22

Giaquinta M, Giusti E (1985) Researches on the equilibrium of masonry structures. Arch Ration Mech Anal 88:359–392. https://doi.org/10.1007/BF00250872

Giordano A, De Luca A, Mele E, Romano A (2007) A simple formula for predicting the horizontal capacity of masonry portal frames. Eng Struct 29:2109–2123. https://doi.org/10.1016/j.engstruct.2006.10.011

Giordano N, Crespi P, Franchi A (2017) Flexural strength-ductility assessment of unreinforced masonry cross-sections: analytical expressions. Eng Struct 148:399–409. https://doi.org/10.1016/j.engstruct.2017.06.047

Giordano N, De Luca F, Sextos A (2020) Out-of-plane closed-form solution for the seismic assessment of unreinforced masonry schools in Nepal. Eng Struct. https://doi.org/10.1016/j.engstruct.2019.109548

Giuffré A (1996) A mechanical model for statics and dynamics of historical masonry buildings. Protection of the architectural heritage against earthquakes. Springer, Vienna, pp 71–152

Gkimprixis A, Tubaldi E, Douglas J (2019) Comparison of methods to develop risk-targeted seismic design maps. Bull Earthq Eng 17:3727–3752. https://doi.org/10.1007/s10518-019-00629-w

Gobbin F, de Felice G, Lemos JV (2021) Numerical procedures for the analysis of collapse mechanisms of masonry structures using discrete element modelling. Eng Struct 246:1147. https://doi.org/10.1016/j.engstruct.2021.113047

Griffith MC, Lam NTK, Wilson JL, Doherty K (2004) Experimental investigation of unreinforced brick masonry walls in flexure. J Struct Eng 130:423–432. https://doi.org/10.1061/(ASCE)0733-9445(2004)130:3(423)

Jaramillo J (2002) Mecanismo de transmisión de cargas perpendiculares al plano del muro en muros de mampostería no reforzada. Revista De Ingeniería Sísmica 53:1. https://doi.org/10.18867/ris.67.205

Lagomarsino S (2015) Seismic assessment of rocking masonry structures. Bull Earthq Eng 13:97–128. https://doi.org/10.1007/s10518-014-9609-x

Lourenço PB, Gaetani A (2022) Finite element analysis for building assessment: advanced use and practical recommendations. ISBN 9781032228396, Routledge, p 422

McGuire RK (2008) Probabilistic seismic hazard analysis: early history. Earthq Eng Struct Dyn 37:329–338. https://doi.org/10.1002/eqe.765

Menon A, Magenes G (2008) Out-of-plane seismic response of unreinforced masonry: definition of seismic input. Report. IUSS Press, ROSE School ISBN: 978-88-6198-021-1

Morandi P, Magenes G, Griffith M (2008) Second order effects in out-of-plane strength of unreinforced masonry walls subjected to bending and compression. Austral J Struct Eng

Moré JJ (1978) The Levenberg–Marquardt algorithm: implementation and theory. In: Watson GA (ed) Numerical analysis, Lecture Notes in Mathematics 630, Springer, pp. 105–116

NTC IM of I and (2018) Norme Tecniche per le Costruzioni. DM 17/1/2018. Gazzetta Ufficiale della Repubblica Italiana

Parisi F, Augenti N (2013) Assessment of unreinforced masonry cross sections under eccentric compression accounting for strain softening. Constr Build Mater 41:654–664. https://doi.org/10.1016/j.conbuildmat.2012.12.039

Parisi F, Sabella G, Augenti N (2016) Constitutive model selection for unreinforced masonry cross sections based on best-fit analytical moment-curvature diagrams. Eng Struct. https://doi.org/10.1016/j.engstruct.2015.12.036

Parisse F, Cattari S, Marques R et al (2021) Benchmarking the seismic assessment of unreinforced masonry buildings from a blind prediction test. Structures 31:982–1005. https://doi.org/10.1016/j.istruc.2021.01.096

Paulay T, Priestly MJN (1992) Seismic Design of Reinforced Concrete and Masonry Buildings. John Wiley & Sons Inc, Hoboken

Simões AG, Bento R, Lagomarsino S et al (2020) Seismic assessment of nineteenth and twentieth centuries URM buildings in Lisbon: structural features and derivation of fragility curves. Bull Earthq Eng 18:645–672. https://doi.org/10.1007/s10518-019-00618-z

Sorrentino L, D'Ayala D, de Felice G et al (2016) Review of out-of-plane seismic assessment techniques applied to existing masonry buildings. Int J Arch Herit 1:1–20. https://doi.org/10.1080/15583058.2016.1237586

Vamvatsikos D (2013) Derivation of new SAC/FEMA performance evaluation solutions with second-order hazard approximation. Earthq Eng Struct Dyn 42:1171–1188. https://doi.org/10.1002/eqe.2265

Woessner J, Laurentiu D, Giardini D et al (2015) The 2013 European seismic hazard model: key components and results. Bull Earthq Eng. https://doi.org/10.1007/s10518-015-9795-1